SAE INTERNATIONAL

ARTICLE INFO
Article ID: 03-16-05-0038

doi:10.4271/03-16-05-0038

Investigation of Ducted Fuel Injection Implementation in a Retrofitted Light-Duty Diesel Engine through Numerical Simulation

Andrea Piano,[1] Cristiano Segatori,[1] Federico Millo,[1] Francesco Concetto Pesce,[2] and Alberto Lorenzo Vassallo[2]

[1]Politecnico di Torino, Energy Department, Italy
[2]PUNCH Torino S.p.A., Italy

Abstract

Ducted Fuel Injection (DFI) is a concept of growing interest to abate soot emissions in diesel combustion based on a small duct within the combustion chamber in front of the injector nozzle. Despite the impressive potential of the DFI proven in literature, its application for series production and the complexity for the adaptation of existing Compression-Ignition (CI) engines need to be extensively investigated. In this context, the aim of this study is to numerically assess the potential of DFI implementation in a CI engine for light-duty applications, highlighting the factors which can limit or facilitate its integration in existing combustion chambers.

The numerical model for combustion simulation was based on a One-Dimensional/Three-Dimensional Computational Fluid Dynamics (1D/3D-CFD) coupled approach relying on a calibrated spray model, extensively validated against experimental data. Once the coupling procedure had been assessed by comparing the numerical results with experimental data of in-cylinder pressure and heat release rate for both low- and high-load operating conditions, the effect of the duct was investigated by introducing it in the computational domain. It was observed that DFI did not yield any significant advantage to engine-out soot emissions and fuel consumption with the existing combustion system. Although soot formation was generally reduced, the soot oxidation process was partially inhibited by the adopted duct keeping the fixed engine calibration, suggesting the need for a complete optimization of the combustion system design. On the other hand, a preliminary variation of engine calibration highlighted several beneficial trends for DFI, whose operation was improved by a simplified injection strategy.

The present numerical results indicate that DFI retrofit solutions without specific optimization of the combustion system design do not guarantee soot reduction. Nevertheless, there is still much room for improvement in terms of DFI-targeted combustion chamber design and engine calibration to achieve the full success of this technology for soot-free CI engines.

History

Received: 29 Jun 2022
Revised: 23 Sep 2022
Accepted: 14 Nov 2022
e-Available: 30 Nov 2022

Keywords

Ducted fuel injection, Diesel engine, Soot mitigation, Computational fluid dynamics, Mixing, Spray

Citation

Piano, A., Segatori, C., Millo, F., Pesce, F. et al., "Investigation of Ducted Fuel Injection Implementation in a Retrofitted Light-Duty Diesel Engine through Numerical Simulation," *SAE Int. J. Engines* 16(5):643-661, 2023, doi:10.4271/03-16-05-0038.

ISSN: 1946-3936
e-ISSN: 1946-3944

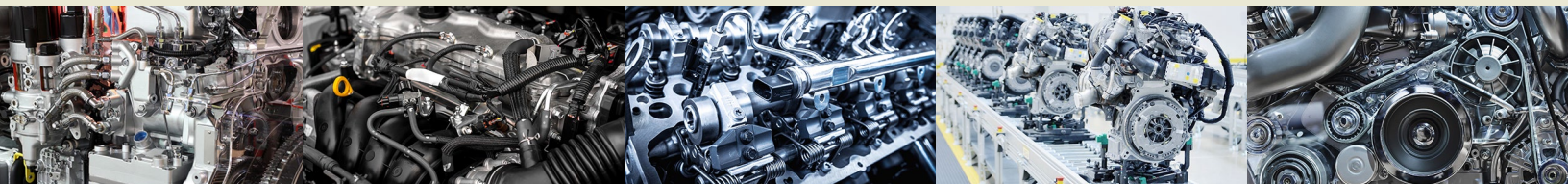

1. Introduction

The Compression-Ignition (CI) engine based on conventional Mixing-Controlled (MC) diesel combustion represents a technically viable (e.g., high specific power, durability and reliability, high controllability), low cost (e.g., compatible with existing fuels infrastructure, abundant and inexpensive materials), energy secure (e.g., high efficiency, compatible with domestic fuels), and climate secure (e.g., compatible with alternative/oxygenated fuels) technology for the transportation of people and goods. These characteristics make CI engines account for a large share of the market still today. For instance, more than 90% of both marine engines sold globally in 2019 [1] and truck engines sold in Europe in 2020 [2] were CI diesel engines. Nevertheless, on-road and off-road diesel engines are among the major sources of anthropogenic soot (i.e., black carbon) emissions [3], for which the whole transportation sector (including international shipping) contributes about 25% worldwide [4]. In the literature, there is well-documented evidence that exposure to soot has adverse effects on human beings [5, 6, 7]. Furthermore, soot is classified as a short-lived climate pollutant, whose reduction could play a crucial role in the mitigation of the near-term climate change [8]. In particular, soot is estimated to have a global warming potential 3200 times higher than Carbon Dioxide (CO_2) over a 20-year time frame [9].

In this context, significant efforts in the diesel research community are presently focused on the curtailing of soot emissions from MC diesel combustion [10], aiming to reduce the fuel-to-air ratio in the autoignition zone to enable the so-called Leaner Lifted-Flame Combustion (LLFC) [11, 12]. Among the various solutions under analysis, increasing interest is captured by the Ducted Fuel Injection (DFI), a very promising concept, patented by Sandia National Laboratories [13], and presently investigated by several academic and industrial research groups across the world.

DFI involves injecting fuel down the axis of a small duct in the combustion chamber that is assembled coaxially to the injector nozzle, with a small gap (named *stand-off distance*) between the duct and the nozzle. The initial experimental analysis in Constant-Volume Combustion Vessel (CVCV) executed by Mueller et al. in [14] compared the soot Natural Luminosity (NL) of DFI with respect to the free spray (i.e., conventional spray configuration without duct) considering Spray A Engine Combustion Network (ECN) conditions [15], showing a notable Lift-Off Length (LOL) extension and an impressive soot abatement over a large air temperature range. The subsequent work by Gehmlich et al. [16] evaluated the soot mass through optical thickness measurements in similar working conditions, confirming that DFI can attenuate soot formation by more than an order of magnitude in comparison with Conventional Diesel Combustion (CDC). Despite this demonstration of dramatic reduction of soot, the involved physical mechanisms were—and still are—not completely clear. Therefore, Computational Fluid Dynamics (CFD) tools have been involved to investigate the effects of the duct adoption on the spray characteristics, under both non-reacting and reacting conditions. Nilsen et al. [17] calibrated a spray model considering Spray A ECN non-reacting conditions and showed a significant in-duct pressure reduction for DFI, which is able to increase the air entrainment at the duct inlet, as well as an equivalence ratio decrease in the expected LOL region. Millo et al. [18] explored the DFI-enabled soot formation mitigation mechanisms, showing an increase of the air entrainment into the fuel spray upstream of the duct, and a remarkable turbulent mixing enhancement in a two-stage process: inside the duct and downstream of the duct. As a result, the equivalence ratio was strongly mitigated and homogenized for DFI on the whole spray area. These mechanisms were then investigated in reacting conditions to understand, on one hand, the influence of the main duct geometrical features (i.e., length, stand-off distance, diameter, and shape) [19] and, on the other hand, the impact of the main engine operating parameters (rail pressure, air density, oxygen concentration, and duct temperature) [20] on DFI performance. Focusing on the latter work, the duct adoption emerged to be synergetic with rail pressure increase in terms of soot reduction due to the dramatic rise of entrainment and mixing mechanisms. However, high air density conditions negatively affect DFI, mainly due to the noticeable LOL shortening, increasing the risk of in-duct ignition.

Even though the available knowledge about DFI working mechanisms is growing and the soot mitigation potential is extremely promising, the translation of this information to its application on CI engines could not be immediate, considering the intrinsic difference between CVCV and real engines. Nilsen et al. [21] carried out the first analysis of DFI on a CI optical access engine, providing evidence that DFI achieves similar benefits in an engine application. A two-hole fuel injector was employed, testing only in a low-load condition (gross Indicated Mean Effective Pressure [IMEP] lower than 3 bar). This investigation was then extended in [22] over a wide range of operating conditions and at higher loads (up to 8.5 bar gross IMEP), employing a four-hole fuel injector. A dilution sweep demonstrated that DFI is capable to break the soot/NOx trade-off typical of CDC, leading to a simultaneous reduction of soot and NOx emissions. This was made possible by enabling DFI to run at lower oxygen concentration levels, usually not feasible with CDC due to high soot emissions. In a subsequent study [23], the focus was shifted to the idle (1.1 bar gross IMEP) and higher load (10 bar gross IMEP) conditions. At idle, DFI confirmed the simultaneous reduction of soot and NOx engine-out emissions. At higher loads, DFI showed only a 27% relative reduction of engine-out soot, despite a more than 70% relative reduction in terms of spatial integral NL. The late-formed soot was deemed responsible for this increase in engine-out soot, due to the lower temperatures and less residual time to oxidize it. Furthermore, jet-jet interaction and entrainment of hot combustion products could play a role, correlating with increased injection pressure and longer injection duration. Finally, they concluded that DFI may require a different calibration than CDC to achieve optimal results. An additional study in an optical research engine (operated in a skip-fired mode) from Wilmer et al. [24]

provided the first measurements of solid Particulate Number (PN). DFI resulted in a reduction in PN for particles larger than 23 nm by 77% compared to CDC, at 13.3 bar gross IMEP. Moreover, the geometric mean diameter of accumulation mode particles was reduced by 26%, suggesting that DFI has the potential to enable fuel savings by lowering the frequency of particulate filter regeneration.

All these studies were conducted on optical research engines; nonetheless, significant differences can emerge when a series production diesel engine is considered. Only one research study from Svensson et al. [25] tested DFI on a heavy-duty metal engine equipped with a six-hole injector, comparing performance and emissions for DFI and CDC at high loads (up to IMEP higher than 20 bar) to evaluate whether DFI could be successfully retrofitted into a production-like combustion system. DFI generally yielded higher engine-out soot emissions, and some speculations were done about the underlying reasons behind this countercurrent outcome: the LOL shortening, due to the re-entrainment of hot combustion products, and the poor soot oxidation, due to jet-jet interaction. Moreover, the worsening of DFI performance with respect to previous studies can also be motivated by the increased number of injector nozzles. High sensitivity to the injection timing was also found. In the end, they concluded that it cannot be assumed that DFI can be retrofitted onto existing engines, which are highly optimized to meet current emission regulations for CDC. On the contrary, the optimization of the combustion system should be considered also for DFI application. Notwithstanding these initial findings, several research questions remain unanswered about the direct retrofit approach of DFI into existing CI engines since it is not clear what factors can limit or facilitate the achievement of this target, from both engine calibration and design perspectives. In light of this, a CFD investigation on the impact of duct adoption on the flow field, combustion, and soot formation and oxidation processes can be of paramount importance, as well as a preliminary understanding of the impact of the injection strategy on the DFI performance.

Therefore, in this article, an existing series production CI engine for light-duty applications was considered to assess the DFI retrofit suitability in both part-load and full-load conditions and to better analyze its potential across the whole engine map. A CI engine model, developed by means of a One-Dimensional/Three-Dimensional (1D/3D)-CFD coupling methodology, was validated against experimental data related to both spray characteristics and in-cylinder combustion parameters (coming from the test bench). Detailed chemistry solver and detailed soot modeling, relying on the soot precursors, were employed to obtain reliable results for both the combustion process and the soot mass. The comparison between CDC and DFI made it possible to analyze the impact of the duct adoption on several in-cylinder physical characteristics, like bulk fluid motions and temperature distributions before the injection, and on the combustion and soot results, during both formation and oxidation phases. Finally, a variation of the injection strategy was considered in part-load conditions, bringing out the potential of a DFI-oriented engine calibration on the final DFI performance.

2. Methodology

2.1. Overview

Since the aim of this study is to numerically assess the potential of DFI implementation in a CI engine, a thoroughly modeled diesel combustion is mandatory. The 3D-CFD modeling approach was adapted from the procedure already published by Millo et al. in [26], in which the 1D- and 3D-CFD environments were coupled. For the present work, the commercially available software CONVERGE CFD was employed for the 3D-CFD analysis, while the GT-SUITE software for the 1D-CFD simulations.

In dealing with CI engine 3D-CFD combustion simulation, the combustion chamber can be divided into a finite number of sectors, equal to the number of nozzle holes, assuming axial symmetry characteristics of the combustion process. This allows for reducing the computational effort by about an order of magnitude, maintaining similar accuracy [27, 28]. However, to reliably implement this approach, proper initialization of the charge motion, thermodynamic variables, and species concentrations becomes crucial to ensure realistic conditions encountered by the spray at the Start of Injection (SOI) timing. Therefore, a preliminary full-cylinder simulation without combustion (named henceforth *Cold flow*) was carried out to obtain an appropriate variable mapping for the sector initialization at the Intake Valve Closure (IVC). The entire cold engine cycle was simulated, setting the inflow and outflow boundary conditions (at the intake and exhaust port, respectively) according to the pressure, temperature, and species concentration traces coming from an already calibrated 1D-CFD engine model. Coming to the sector initialization at IVC, due to the effect of intake and exhaust flows on the in-cylinder charge, the eight available sectors showed slight differences: the sector characterized by the closest mean values to the cylinder was selected for this analysis to ensure the best whole field representation. It is noteworthy that the sector simulation approach is valid also for DFI simulations because the axial symmetry is guaranteed.

In addition, the implementation of a high-fidelity spray model is also an aspect of paramount importance to achieve a good predictive capability of the 3D-CFD CI engine model. Hence, a 3D-CFD spray model was preliminarily calibrated and validated against experimental data from the constant-volume test vessel.

Finally, the 1D-CFD environment was again exploited to post-process the 3D-CFD combustion simulation results by means of the Cylinder Pressure–Only Analysis, previously used to post-process experimental data. The usage of the same post-processing tool for both experiments and simulations allowed them to be compared consistently, under some assumptions.

2.2. Spray Characterization

The spray model was developed taking advantage of available experimental data. Indeed, an extensive experimental

campaign characterized the injection in evaporative conditions employing a Mie-scattering technique in an optically accessible test vessel. Stabilized Liquid Length (LL) values were thus obtained for several operating conditions, averaging the data coming from the eight holes on seven repetitions (i.e., 56 samples), at different rail pressure, air density, and air temperature. Additional information on maximum mass flow rate, effective diameter, and effective velocity was also provided by momentum measurements, carried out by means of a piezo-electric force sensor.

From an overall point of view, the spray model details are summarized in Table 1.

Focusing on the grid settings, a Cartesian mesh was employed with a base grid size equal to 2 mm and a minimum grid size equal to 0.25 mm, ensuring grid convergence. The minimum grid size was achieved using the Adaptive Mesh Refinement (AMR) algorithm [35], which is able to refine the mesh where needed according to velocity gradients.

A correlation plot representing the calibrated spray model outcomes in terms of LL compared with the experimental ones is reported in Figure 1.

From a general perspective, the 3D-CFD results were deemed accurate enough with respect to the experimental data, given the low prediction error in most of the cases and the main trends with rail pressure (empty vs filled symbols), air density (shape variations), and air temperature (color variation) always captured. Furthermore, considering the 900 K temperature condition for which the simulation accuracy tends to decrease, the largest prediction error is associated with a high density–low rail pressure operating condition (red filled square), which is atypical for CI engine operation, where air density and rail pressure are typically correlated. Therefore, the calibrated 3D-CFD spray model was considered representative of the injection behavior characterizing this case study and, thus, was employed for the subsequent development of the CI engine model.

2.3. CI Engine Model

As mentioned above, the CI model was developed by coupling the 3D-CFD environment with 1D-CFD models for accurate boundary conditions initialization, and standardized and consistent post-processing analysis.

TABLE 1 3D-CFD spray model setup.

Injected fuel (liquid)	Diesel #2
Evaporating species	N-heptane (N-C_7H_{16})
Turbulence model	RANS–RNG k-ε [29]
Liquid injection	Blob model [30]
Droplet turbulent dispersion	O'Rourke model [27]
Spray breakup	KH-RT model [31]
Evaporation	Frossling with boiling model [27]
Droplet drag	Dynamic drop and drag [32]
Spray/wall interaction	Rebound/slide model [33]
Heat transfer	O'Rourke and Amsden model [34]

FIGURE 1 LL correlation plot between experimental data and simulation results for several operating conditions varying in terms of air density (symbol shape), rail pressure (symbol filling), and air temperature (symbol color).

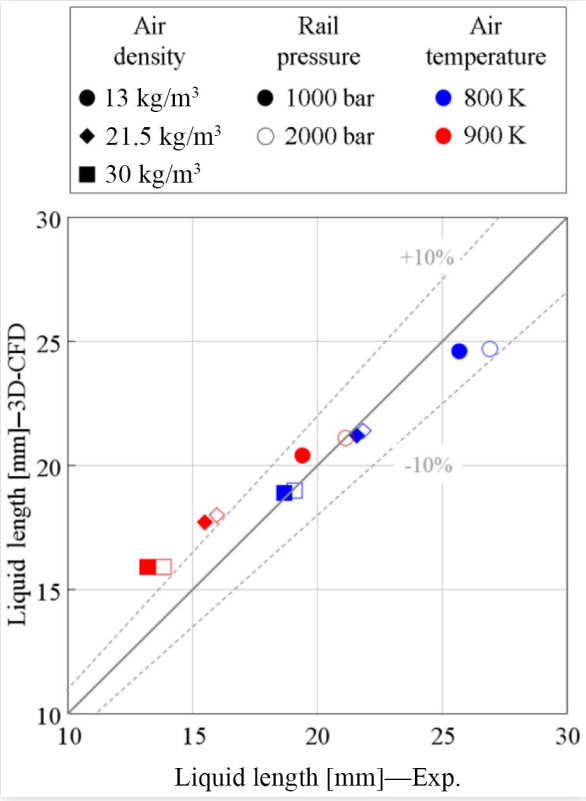

In dealing with the 3D-CFD environment, two steps were carried out: full-cylinder cold flow simulation and sector combustion simulation. The latter was initialized at the IVC with variables mapping coming from the former and featured the calibrated spray model analyzed in the previous paragraph.

The experimental data for model validation purposes were provided by an experimental campaign at the test bench on a series production CI engine, whose specifications are reported in Table 2. This engine, adopted for light-duty applications, is characterized by a unit cylinder displacement of approximately 0.8 L. It is equipped with a common rail fuel injection system, featuring an 8-hole injector with a hole diameter of about 0.140 mm, and a sharp-step re-entrant piston bowl.

Three different working points (i.e., *K-points*), reported in Table 3, were selected for the analysis. These characterize

TABLE 2 CI engine specifications.

Application	Light-duty vehicles
Displacement	≈0.8 L
Bore/stroke	≈1

TABLE 3 Engine working points.

Engine speed n [rpm]	Brake mean effective pressure BMEP [bar]
1800	6
2000	17
2800	≈23 (full load)

both low-load and high-load operating conditions. It is noteworthy that the data were collected only for the free spray configuration, while no experimental data were available for the DFI configuration.

Moving to the 3D-CFD case setup, the main characteristics of both full-cylinder and sector simulations are summarized in Table 4.

The computational domain was meshed in both cases with a patented cut-cell technique [35] generating a Cartesian grid. Several embeddings for localized mesh refinements were adopted in critical areas for the flow motion and heat exchange. A minimum grid size of 0.25 mm was reached in both full-cylinder and sector simulations, enabling the AMR algorithm based on velocity and temperature gradients. It is noteworthy that the minimum grid size is the same as the above-discussed spray simulations, thus ensuring a good prediction of the spray penetration. A sketch of the mesh adopted for full-cylinder cold flow simulation and sector simulation during the intake phase and the fuel injection phase, respectively, is reported in Figure 2. For the sake of completeness, the sketch is referred to the DFI case, when further embedding in the duct region to ensure a reasonable number of cells inside the duct is employed.

Finally, the combustion simulation outcomes are reported in Figure 3 for each considered K-point, compared to the experimental data in the form of correlation plots. In particular, the main combustion parameters are evaluated for combustion anchor angle (i.e., MFB50), combustion duration (i.e., MFB10-75), and maximum pressure value and its phasing. As mentioned above, this comparative analysis can be performed only for the free-spray configuration.

TABLE 4 3D-CFD setup summary for both full-cylinder (cold flow) and sector combustion simulations.

	Full cylinder (*Cold flow*)	Sector
Simulation window	From EVO to TDCf	From IVC to EVO
Turbulence model	RANS–RNG k-ε [29]	RANS–RNG k-ε [29]
Heat transfer model	O'Rourke and Amsden model [34]	O'Rourke and Amsden model [34]
Spray model	\	Calibrated spray model (Table 1)
Combustion model	\	SAGE detailed chemistry solver
Chemical kinetics	\	Skeletal Zeuch mechanism [36] with PAHs (A3R5-) as soot precursors and thermal NOx reactions
Soot formation/ oxidation	\	Particulate Mimic model [37]

FIGURE 2 Mesh adopted for full-cylinder cold flow simulation (top) and sector combustion simulation (bottom), in DFI configuration, during intake phase and fuel injection phase, respectively.

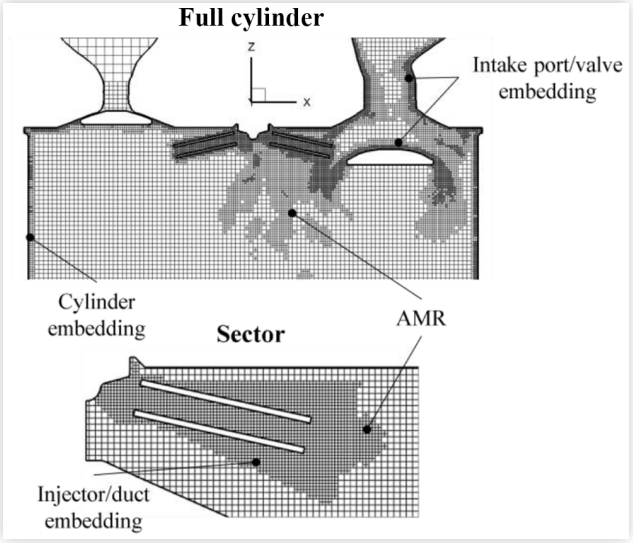

FIGURE 3 Main combustion parameters correlation plots between experimental data and simulation results: MFB50 (a); MFB10-75 (b); pressure peak value (c); crank angle at pressure peak value (d). Working points: 1800 rpm × 6 bar (red circles); 2000 rpm × 17 bar (red diamonds); 2800 rpm × full load (red squares).

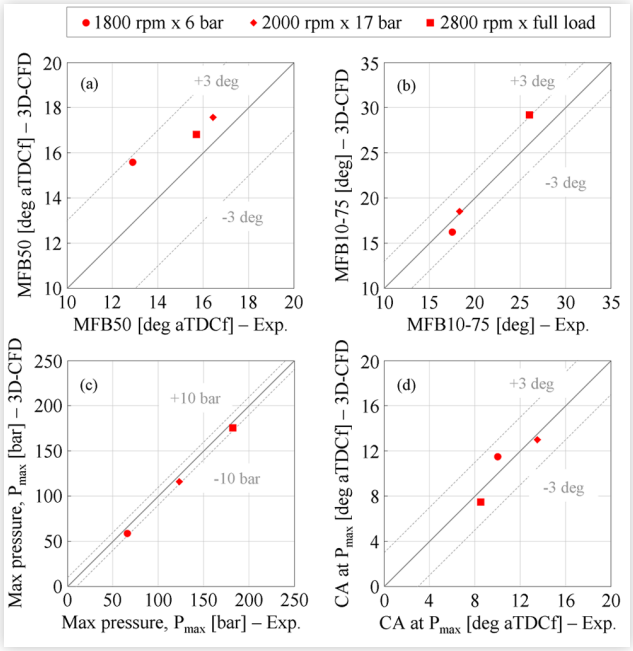

A general good agreement can be observed between numerical simulations and experimental data. Indeed, all the numerical results fall in the acceptable range of absolute deviation, showing a good predictivity of the model. A slight overestimation of the MFB50 (Figure 3(a)) is present, especially for the 1800 × 6 K-point (red circle), due to the longer Ignition Delay (ID) predicted by the combustion model. However, since it marginally affects the overall behavior, as shown by the pressure peak value and phasing (Figure 3(c, d)), and by the combustion duration (Figure 3(b)), this prediction error can be considered negligible. Thereby, according to the present results, the CI model was considered validated for the free-spray configuration.

2.4. DFI Configuration

As far as the DFI configuration is considered, the duct geometry was simply implemented in the computational domain and modeled according to the available knowledge, without any validation against experimental data. However, although the DFI analysis should be considered fully predictive, reliable information is expected by this modeling approach. In fact, concerning the impact of the duct adoption on the spray model, the available literature showed that no modifications seem needed when the Kelvin-Helmholtz Rayleigh-Taylor (KH-RT) breakup model without breakup length is employed [18], and the rebound/slide model is considered for the interaction between the spray and duct wall. Instead, as regards the impact of the duct on the cylinder thermal field and vice versa, a constant duct temperature was considered for this exploratory analysis. This hypothesis can be considered robust since the duct, together with the duct holder (e.g., [22, Figure 5]), would be assembled in the cylinder head and a regime temperature would probably be reached, similar to the other combustion chamber components. More challenging is a reliable estimation of the temperature value at the current knowledge status: for this work, it was fixed equal to the cylinder head. This modeling approach is in line with the assumptions provided by Nilsen et al. [21] and the related error is expected to be relatively small. A more accurate estimation (e.g., by means of conjugate heat transfer simulation) was out of the scope of this exploratory analysis and will be the object of future works.

Concerning the duct design, a sharp inlet–sharp outlet duct, perfectly aligned with the injector nozzle, was assumed. In particular, the D2L14G3 geometry with a wall thickness of 0.5 mm was considered, characterized by an internal diameter (D) of 2 mm, a length (L) of 14 mm, and a stand-off distance (G) of 3 mm. A sketch of the adopted duct geometry is reported in Figure 4.

This duct design is a slight modification of the D2L14G2, which is a reference geometry in the scientific literature on DFI for several test vessel experiments and CFD simulations [18, 19, 38, 39]. The 1-mm variation of the stand-off distance with respect to the reference case is motivated by the packaging limits when the duct is assembled in the existing combustion chamber. In fact, to avoid interference between ducts and the injector, and between adjacent ducts (considering the high number of injector holes), a minimum stand-off

FIGURE 4 Duct design (D2L14G3) employed for the study (distances in millimeters [mm]).

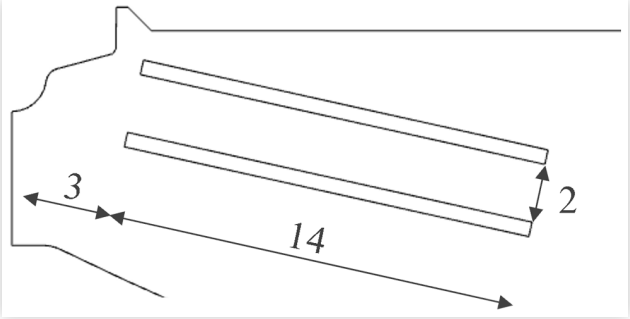

distance of about 2.5 mm was required in this case for the considered duct diameter. The modification of the stand-off distance was preferred to the duct diameter due to the huge effects of the latter on the duct performance, as seen in [19].

Concerning the Compression Ratio (CR), due to the direct retrofit purpose of this work, the variation correlated to the presence of the ducts inside the combustion chamber was neglected, as commented in the next sections.

It is noteworthy that in this preliminary analysis the duct was ideally mounted without any duct holder, whose influence on velocity and thermal fields is thus neglected. Nevertheless, since the duct holder would mainly affect the solid thermal behavior of the duct, which is herein not simulated, its absence is expected to marginally affect the simulation outcome. Future investigations will be focused on the design optimization of the duct holder, also including its thermal analysis.

3. Results: Free Spray vs. DFI

3.1. In-Cylinder Charge Motion

Although the full-cylinder cold flow simulations were carried out with the aim of providing a reliable field initialization for the sector combustion simulations, several insights about the influence of the duct adoption on the fluid bulk motion can be obtained by comparing the results related to free-spray and DFI configurations. These results are qualitatively similar for each considered K-point; thus, for the sake of brevity, only the 2800 rpm at full-load case will be shown.

First of all, the effect of the duct presence on the velocity field at the SOI is analyzed. In Figure 5, the tangential velocity (i.e., the magnitude of the velocity component orthogonal to the cylinder axis) field at SOI on three different sections parallel to the cylinder head is reported for both free spray and DFI. The sections are located at three different distances from the cylinder head: duct inlet (Z1), duct outlet (Z2), and inside the bowl about 2.5 mm under the duct outlet location (Z3).

FIGURE 5 Tangential velocity magnitude field at the SOI for free spray (left) and DFI (right) on sections orthogonal to the cylinder axis at three different heights: duct inlet (Z1), duct outlet (Z2), and inside the bowl (Z3). Working point: 2800 rpm at full load.

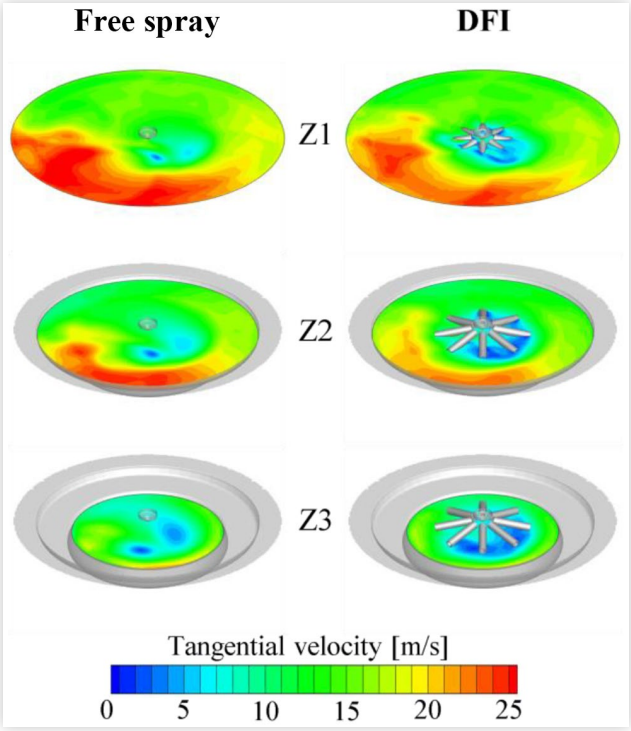

FIGURE 6 DFI swirl ratio normalized with respect to the free-spray one. IVC timing and SOI timing are indicated with vertical dashed lines. Working point: 2800 rpm at full load.

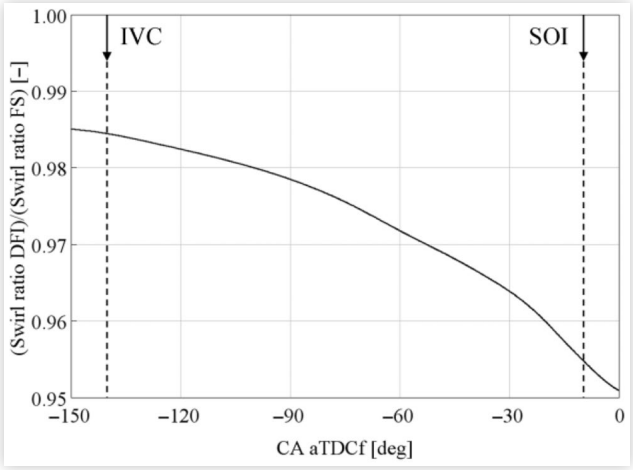

As can be observed, the presence of the ducts inside the combustion chamber significantly affects the flow field, reducing the velocity values, especially in the region closer to the cylinder axis. However, this reduction is also visible in the periphery of the chamber. This is particularly evident at Z1 (Figure 5, top) near the liner and at Z2 (Figure 5, middle) in the piston step region. Focusing on Z3 (Figure 5, bottom), it can be seen that the duct presence reduces the velocity values even inside the bowl. From an overall perspective, this behavior suggests a decrease in the swirl intensity with DFI. In light of this, the DFI swirl ratio normalized with respect to the free-spray one is represented as a function of the Crank Angle (CA) in Figure 6, mainly focusing on the compression stroke.

According to Figure 6, compared to the conventional configuration, the DFI case features a lower swirl intensity due to flow-duct interaction, especially toward the end of the compression stroke, that is, when the duct impact is higher due to the reduced available volume. Since the swirl motion is a crucial parameter for understanding the mixing capability of a certain combustion system design, the abovementioned reduction must be considered as an initial gap in terms of mixing for the DFI configuration, which could weaken the benefits of the DFI mixing.

It is noteworthy that the greater impact of the presence of ducts toward the Top Dead Center (TDC) is not only limited to the reduced swirl ratio but also the in-cylinder trapped mass involved in the duct region should be taken into account. Indeed, an inlet-only flow characterizes the duct region during the compression stroke, leading to the absence of recirculation and progressively larger mass inside the ducts, exchanging heat with the walls. Based on this concept, the duct wall temperature becomes an important parameter to control the local temperature conditions encountered by the spray entering the duct in the DFI configuration. A preliminary sensitivity analysis was performed on this aspect, varying the constant temperature value imposed on the ducts between a lower limit (i.e., head average temperature, 520 K) and an upper limit (i.e., exhaust valve average temperature, 1054 K). In addition, an intermediate value of 780 K has been considered. In Figure 7, the charge gas mass flow rate between the cylinder and ducts during the compression stroke is reported as a function of CA for three different duct wall temperatures on the top graph. On the bottom graph, the average cylinder and in-duct temperature values, as a function of CA, are represented for both free-spray and each DFI case.

Focusing on the cylinder-to-duct mass transfer (Figure 7, top), a positive flow entering the duct can be observed during the compression stroke. The maximum value is reached near the TDC when the piston motion is not already null. A slight dependence on duct wall temperature can also be noted, leading to a larger in-duct mass for lower duct temperature due to higher in-duct local density.

Moving to the average temperature behavior (Figure 7, bottom), the cylinder values (solid lines) are very similar between free-spray (red) and each DFI configuration (blue, green, and magenta). In fact, with the combustion chamber designs being equal, the presence of the ducts leads to a deviation of about 0.1 on the CR, which means only a slightly higher temperature at the end of the compression stroke. At the same time, focusing on the DFI cases, the curves related to the cylinder region are practically overlapped, suggesting that the

FIGURE 7 Charge gas mass flow rate cylinder-to-ducts (top graph) and average temperature (bottom graph) of the cylinder (solid line) and duct region (dashed line) for free-spray (red) and DFI configuration at different imposed duct wall temperature values: 520 K (blue), 780 K (green), and 1055 K (magenta). Working point: 2800 rpm at full load.

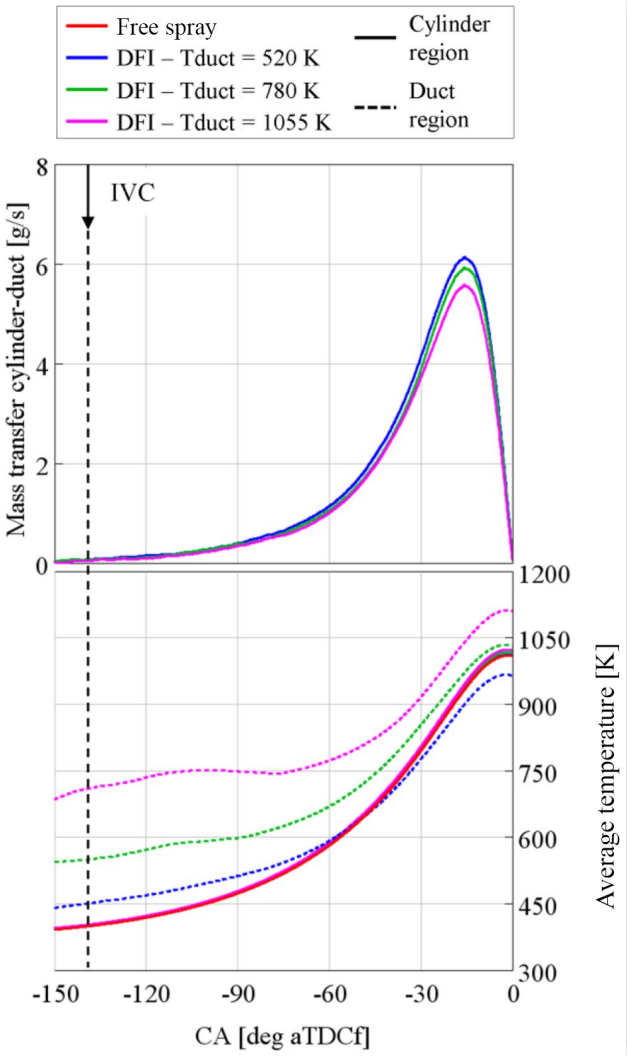

duct wall temperature only marginally affects the average temperature values in the cylinder.

Nevertheless, the conclusions are very different considering the in-duct region. First of all, the in-duct average temperature (dashed lines) is significantly different from the cylinder one, regardless of the imposed duct wall temperature. In particular, at the IVC the temperature of the ducts is 310 K and 150 K higher with respect to the cylinder for the wall temperature of the ducts at 1055 K (magenta) and 780 K (green), respectively. Without any cylinder-to-ducts mass transfer (i.e., closed system), the initial in-duct mass would follow a polytropic compression starting from a different temperature value with respect to the cylinder region. By simply considering this assumption and focusing on the 1055 K duct wall temperature case, the expected in-duct final temperature would be about 1725 K for the initial in-duct mass, clearly overestimated compared with the simulation results. Since the cylinder-to-duct mass transfer plays a huge role and the entering gas features a lower temperature (equal to the cylinder one), a much lower in-duct temperature is expected, according to a mass-weighted temperature balance. Finally, also the fluid-solid heat exchange during the compression stroke plays a role in the definition of the final in-duct temperature value. Since this final value determines the local conditions encountered by the ducted spray at the SOI, potentially affecting the ignition timing and the soot mitigation performance as shown in the thermal boundary layer analysis in [40], thermal management of the duct could be of paramount importance.

According to the herein results, at the SOI an increment of 100 K for the 1055 K duct wall, due to the much higher initial in-duct temperature and the positive solid-to-fluid heat transfer, can be observed. This computed 100 K difference could definitely affect the reactivity of the incoming spray at the SOI. Considering instead the 780 K duct wall, the temperature at the SOI is 30 K higher than the free spray: in this case, given that the in-duct mean temperature is similar to the imposed duct wall temperature, the fluid-solid heat exchange tends to be negligible on average. Therefore, the final increment is caused by the 150 K higher initial in-duct temperature, properly mitigated by the charge gas mass transfer between the cylinder and ducts. Finally, focusing on the 520 K duct wall, the solid-to-fluid heat transfer is negative on average, and the in-duct mass is cooled down during the compression stroke. Furthermore, the initial in-duct temperature increment (about 50 K) is lower than in the other test cases. Thereby, the in-duct temperature at the SOI is even lower than the free-spray configuration (i.e., approximately -40 K), leading to a potential retard of the start of combustion.

It is important to note that these conclusions are strictly related to cold flow analysis, while the inclusion of the combustion process could introduce different aspects, not directly investigable at this stage (e.g., the impact of duct temperature on soot oxidation), which are to be taken into account for a comprehensive and effective duct thermal management.

3.2. K-Point: 1800 rpm × 6 bar

The results of the sector combustion simulations related to the low load K-point are presented in this section, comparing free-spray and DFI configurations. In Figure 8, the fuel injection rate, the burn rate and the in-cylinder pressure, the in-cylinder soot mass trace, and its first derivative (i.e., soot formation/oxidation rate) are reported for both free-spray and DFI configuration as a function of CA.

The injection rate (Figure 8(a), gray) is characterized by two small pilot injections, one main and one post injection. Considering only the amount of fuel injected after the pilot injections, the main and the post injection feature a fuel mass share of about 75% and 25%, respectively. The rail pressure is

FIGURE 8 Fuel injection rate (a), burn rate and in-cylinder pressure (b), in-cylinder soot mass (c), and soot formation/oxidation rate (d) for both free-spray (red) and DFI (blue) configuration. Working point: 1800 rpm at 6 bar.

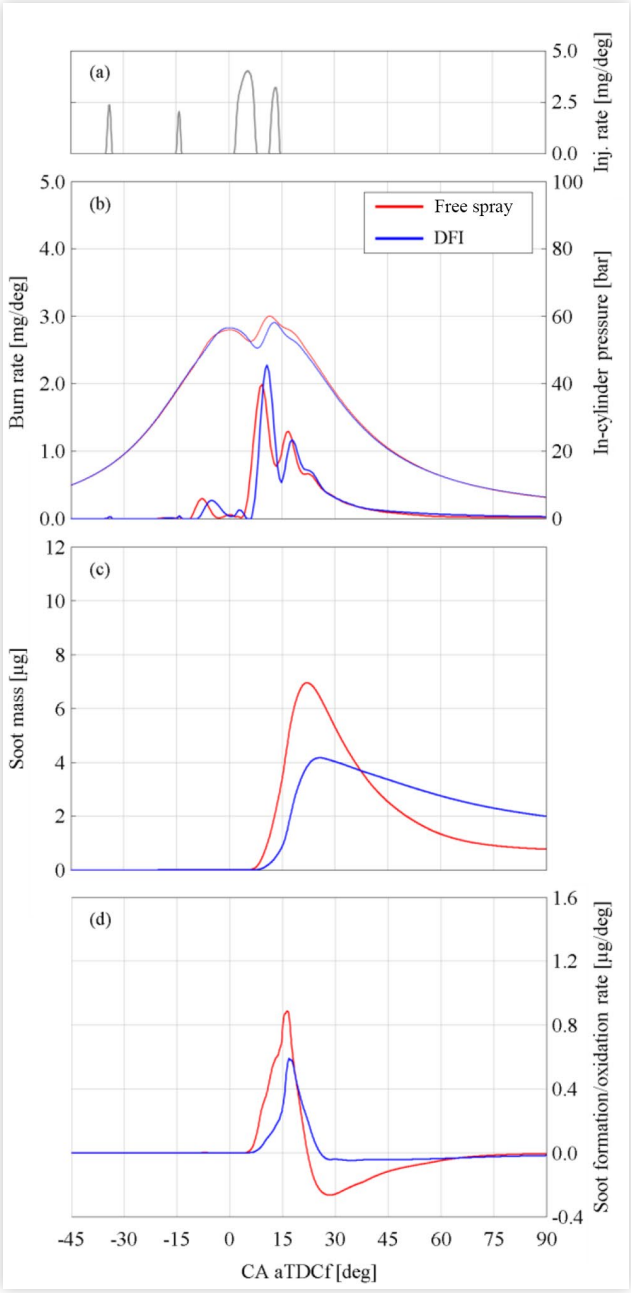

at about 1500 bar. Comparing free spray (red) and DFI (blue) in terms of burn rate (Figure 8(b)), most of the typical trends characterizing DFI combustion can be detected. In fact, the adoption of the duct leads to a longer ID and, consequently, a more intense premixed combustion, as shown by the higher and retarded burn rate peak. On the contrary, the burn rate associated with the post injection combustion is lower than the free spray, despite the retarded ignition. This leads to a slower end of combustion, unusual for DFI technology which typically features a much faster burnout, as analyzed in CVCV [14, 18, 41]. In the end, the abovementioned variations are reflected on the in-cylinder pressure traces (Figure 8(b)), causing a load decrease of about 3% with DFI, for the same injected fuel mass.

The in-cylinder soot mass (Figure 8(c)) shows a retarded rise in the curve and a significantly lower soot mass peak for DFI, highlighting a remarkable reduction of soot formation during the main combustion phase. This is also clear by looking at the soot formation rate curve (Figure 8(d)), which shows much lower values than free spray for the whole injection duration and most of the combustion associated with the main injection. However, moving to the late combustion phase, a higher in-cylinder soot mass is present for DFI due to a strong reduction of the soot oxidation rate compared to the free-spray curve.

Focusing on the soot formation phase, the presence of the duct in the combustion chamber is effective in reducing soot compared to the free spray, despite this mitigation being less impressive than most of the literature on the subject. This difference can be related to several aspects as follows:

- The size of the herein combustion chamber, designed for light-duty applications, which could mitigate the DFI soot mitigation mechanisms with respect to test vessel studies and heavy-duty CI engines.
- The shape of the combustion chamber, which is again optimized for the free-spray configuration and does not take into account the characteristics (e.g., higher penetration) of the ducted spray.
- The engine calibration, which is optimized for free-spray configuration since a direct retrofit methodology was adopted with DFI; thus, no effort was spent in trying to maximize the DFI benefits.

The first two points, being related to geometrical aspects, are not herein investigated but will be objects of future works. The third point is preliminarily analyzed in terms of injection rate shape in a later section. It is noteworthy that since experimental data for validation were not available for DFI configuration, the reduced effectiveness in terms of soot formation could be also related to simulation inaccuracies, especially due to the high level of wall/flow interaction at both the duct wall and the piston rim. However, the usage of the Particulate Mimic model, with soot precursors and soot reactions in the combustion mechanism, ensures the reliability of the model due to its ability to provide accurate quantitative predictions of soot [42].

Focusing on the soot oxidation phase, the negative impact of similar aspects seems even more evident. In fact, the oxidation rate for DFI is much lower than the free spray, as highlighted by the first derivative curves (e.g., DFI soot oxidation rate only a bit lower than 0), leading to higher soot mass toward the Exhaust Valve Opening (EVO) despite the advantage in terms of soot formation.

In order to better understand the soot mass behavior, a local analysis of the 3D results is proposed below, focusing,

first, on the soot formation phase only and then on the soot mass temporal evolution up to the late oxidation phase.

First of all, the DFI soot formation mitigation is investigated, illustrating the equivalence ratio (ϕ) results during the main injection for both the free and ducted sprays on two different combustion chamber sections (Figure 9). The frame is taken at 6 degrees after Top Dead Center firing (deg aTDCf) (i.e., near the maximum of the main injection rate) to be as close as possible to the pseudo-stationary conditions used for the previous analyses in the test vessel [18, 19, 20]. This allows an easier comparison with the DFI analyses in the previous works.

The first section is a vertical plane passing the nozzle and the cylinder axes (Figure 9, top), while the second one is the respective orthogonal plane passing for the nozzle axis (Figure 9, bottom), indicated with the A-A segment. From both sections, it emerges that DFI attenuates the ϕ values, both inside and downstream of the duct. Similar values are only reached where the spray impinges on the piston wall, but the rich area is less extended for DFI. However, this increase in ϕ after the duct exit was not present in the test vessel simulations, suggesting that the spray/bowl interaction could deteriorate the mixing benefits of duct adoption, which is particularly intense after the duct exit according to [20]. In light of this, the relatively small size of this light-duty combustion chamber could be a crucial aspect, and proper optimization of its design should be considered to fully take advantage of the DFI soot formation mitigation mechanisms. Despite this, from an overall point of view, DFI leads to a significant advantage in terms of air-fuel mixing, motivating the soot formation reduction observed in Figure 8.

Similar to the previous works [18, 19, 20], the ϕ distribution can be interpreted by analyzing the entrainment in the fuel spray and the turbulent mixing. The first is evaluated as the charge gas mass flow rate crossing an iso-surface surrounding the spray plume, while the second is evaluated using the Turbulent Kinetic Energy (TKE) along the spray axis as an index. Hence, in Figure 10, the cumulated value of the entrainment along the spray axis and its normalization over the respective iso-surface area (i.e., the so-called mass flux) are reported as a function of the axial distance of the spray, with the TKE along the spray axis (i.e., *centerline TKE*). At the bottom, the ϕ along the spray axis (i.e., *centerline ϕ*) as a function of the axial distance of the spray is also reported. All the graphs are related to the 6 deg aTDCf time instant. For the sake of clarity, a properly scaled sketch of the ducted spray is represented on the top of the figure and a gray band is represented to easily identify the duct axial region.

The cumulated entrainment (Figure 10, top, solid lines) and the mass flux (Figure 10, top, dashed lines) curves can

FIGURE 9 Equivalence ratio distribution during the main injection (6 deg aTDCf) on a vertical section (top) and a respective orthogonal section (A-A, bottom) of the combustion chamber for both free spray (left) and DFI (right). Working point: 1800 rpm at 6 bar.

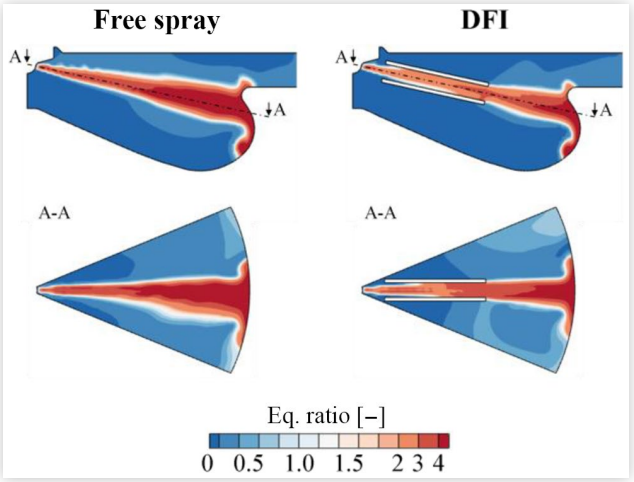

FIGURE 10 Cumulated entrainment (top, solid line) and mass flux into the fuel spray (top, dashed line), centerline turbulent kinetic energy (middle), and centerline equivalence ratio (bottom) during the main injection (6 deg aTDCf) as a function of the axial distance of the spray for both free-spray (red) and DFI (blue) configuration. Working point: 1800 rpm at 6 bar.

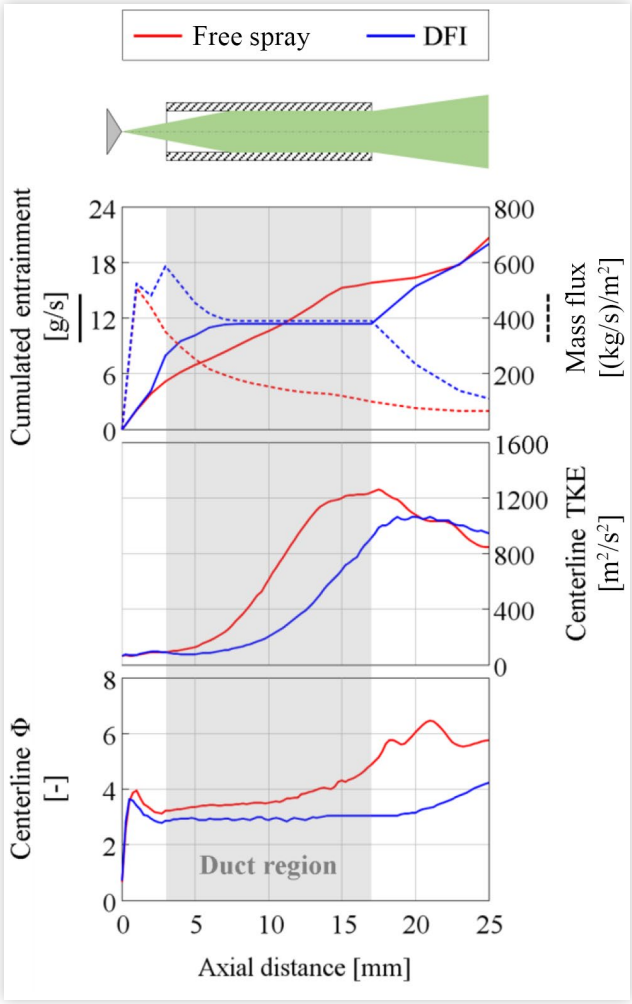

be analyzed by decomposing the distance in three main zones characterizing the DFI configuration: before the spray duct interaction (0–7 mm axial distance); along the collision length (7–17 mm); after the duct exit (17–25 mm).

In the first zone (upstream of the duct), DFI (blue) shows higher entrainment than free spray (red) due to the pumping effect (driven by the in-duct pressure reduction), as deeply analyzed in [17, 18, 19]. The slope of the free-spray curve is relatively constant, leading to linear growth of the cumulated entrainment as the distance from the nozzle increases. On the other hand, after an initial increase with a remarkably higher slope, the DFI curve gradually flattens after the duct inlet due to the progressive spray surface shrinking. Finally, when a collision length is established between the spray and duct wall, the DFI cumulated entrainment becomes constant. However, given the initial entrainment enhancement, DFI features about a 40% advantage with respect to the free spray at a 7 mm axial distance. The DFI advantage is particularly evident in terms of mass flux. Both the free-spray and DFI mass flux curves peak close to the injector nozzle, the most important region for the entrainment [43], and then gradually decrease. However, at the point of contact between the spray and duct, DFI shows an approximately 50% higher value, manifesting that the higher upstream mass flow rate is achieved despite a lower spray surface.

In the second zone (along the collision length), the DFI curve remains constant due to the presence of the duct wall which zeroes the mass flow rate contribution. Instead, the free spray increases at a rate similar to the previous zone, thus overcoming the DFI. The breakeven point is reached at about 12 mm axial distance, in the second half of the duct length. At the duct exit, DFI features about 30% lower cumulated entrainment. It is noteworthy that also the mass flux remains constant for DFI along the collision length because no spray surface is exposed to the surrounding gas. On the other hand, the free-spray mass flux decrease since the entrainment intensity is progressively lower moving away from the nozzle region (e.g., due to lower spray velocity) and the surface contribution tends to increase due to the spray cone enlargement.

In the third zone (downstream of the duct), the high-velocity gradients characterizing the ducted spray at the duct exit [18, 19] lead initially to a much higher local entrainment for DFI, making it rapidly close the gap with the free spray in terms of cumulated value. At 25 mm axial distance, a similar total cumulated value is reached for free spray and DFI. Nevertheless, the global mass flux, computed in the same location, is higher for DFI due to a similar mass flow rate crossing a smaller spray surface.

This mass flux and cumulated entrainment computations support the idea that the presence of the duct, on one hand, enhances the entrainment intensity and, on the other hand, changes its distribution along the spray axis. In fact, even if the entrained gas is equal from a global perspective, it is important to point out that the higher amount of mass entering the spray in the zone close to the injector tip (DFI case) is much more beneficial, as highlighted in [20], due to the longer available mixing length before the ignition. While upstream entrainment is enhanced, the downstream one is slightly lower for DFI, considering that the free spray does not feature a collision length. This is in line with the analysis in [20], where the air entrainment downstream of the duct was similar (or even lower) to the free-spray one when the mixing length (or LOL) was too short. In this case, the geometrical constraints (spray/bowl interaction) and the different injector characteristics reduce the DFI mixing length advantage, presumably determining this downstream entrainment reduction.

Moving to the centerline TKE (Figure 10, middle), the free spray shows a higher turbulent mixing than DFI up to 20 mm, thus including the whole duct region, while the curves reach similar values toward the spray tip, with slightly larger values for DFI, similarly to the findings in [38]. The centerline value can be considered representative of the spray cross section at a certain axial distance since a high radial homogenization level is present. In this case study, this applies also to the DFI configuration, whose behavior is thus different from those observed in previous works [18, 19], for which the radial distribution was of paramount importance. In particular, the two-stage turbulent mixing enhancement (inside the duct and after the duct exit), arising from the interaction between the spray and duct wall, is not present in this case. The herein different behavior could be correlated to the different injector employed for this analysis, which features a lower nozzle diameter and high evaporation and breakup tendency. In light of this, the resulting lower spray liquid fraction through the duct could affect the turbulent mixing enhancement mechanism detected in previous analyses. Indeed, a lower liquid fraction tends to decrease the ducted spray momentum conservation which is the prime mover of the turbulent regime inside the duct and the formation of vortex rings due to high-velocity gradients at the duct exit, which work as a trigger for the so-called second-stage turbulent mixing.

Finally, the resulting centerline ϕ (Figure 10, bottom) can be observed. DFI is characterized by a remarkable ϕ reduction overall, manifesting that the upstream entrainment plays a major role in this case study. It is worth noting that, although it is consistent with several works [14, 17, 18], this ϕ outcome contradicts the local mixture fraction measurements in [44], indicating a richer spray centerline exiting the duct. This manifests how the different injection and thermodynamic conditions can drastically change the DFI behavior and its predominant soot mitigation working mechanisms, highlighting the still-needed investigations for comprehensively understanding this technology.

Although DFI leads to a soot formation reduction, Figure 8 has shown that higher engine-out soot emissions are caused by the adoption of the duct due to its negative impact on soot oxidation in this case study. To better understand the underlying reasons behind this outcome, a time-varying local analysis is needed. Therefore, in Figures 11 and 12, correspondingly the temperature and soot mass distributions on a section of the combustion chamber, passing the cylinder and nozzle axes, are reported for both free spray and DFI at different selected time instants.

FIGURE 11 Temperature distribution on a vertical section of the combustion chamber for both free spray (top) and DFI (bottom) configuration at different time instants (from left to right). Working point: 1800 rpm at 6 bar.

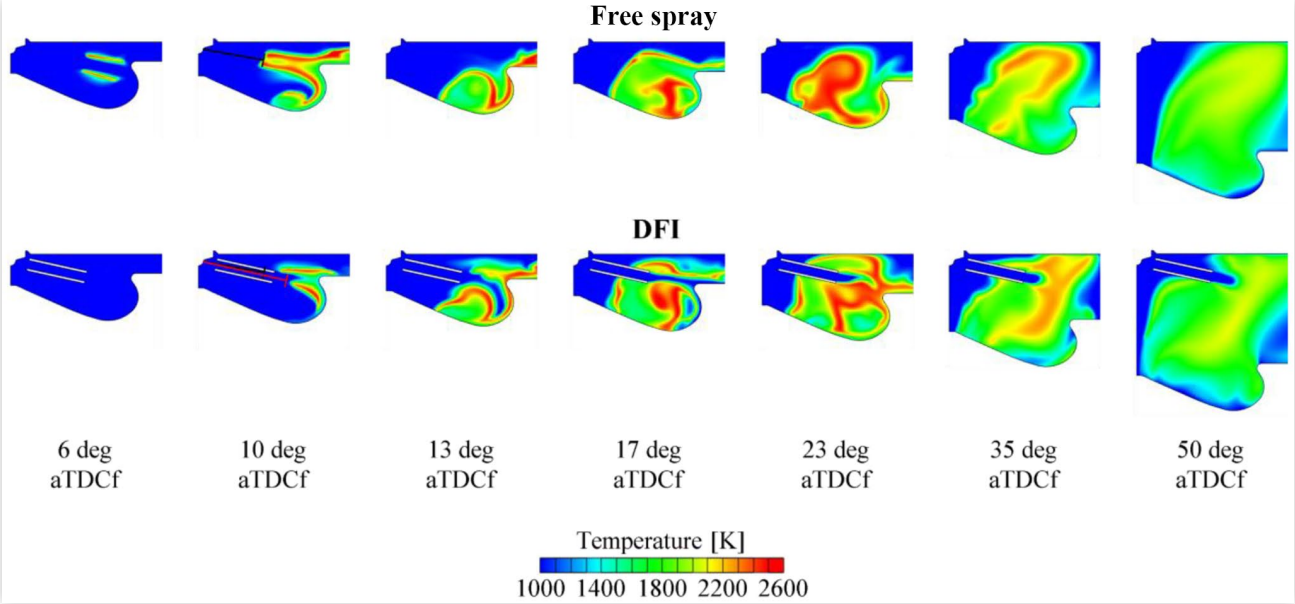

- **6 deg aTDCf**: This time instant relates to the main injection at its maximum fuel mass flow rate previously analyzed. For the free-spray case, a temperature increase due to ignition can be observed on the periphery of the spray, while the abovementioned longer ID is confirmed for DFI, where no ignition is highlighted. The soot has practically not yet formed in both configurations, as confirmed in Figure 8.
- **10 deg aTDCf**: This time instant relates to the combustion of the main injection during the dwell time between the main injection and post injection. Stabilized spray flames can be observed, featuring the LOLs highlighted with black and red segments for free spray and DFI, respectively. The duct adoption leads to a significant extension of the LOL, ensuring DFI works properly, without in-duct combustion. From an overall perspective, the flame area is less extended and the temperatures lower for DFI. In terms of soot mass, soot pockets can be noted inside the bowl and near the step region for the free spray, while quasi-zero soot is depicted for DFI.
- **13 deg aTDCf**: This time instant relates to the post injection at its maximum fuel mass flow rate. This fuel mass is injected during the main-injection-related combustion. It is immediate to note that the post injection must react in a colder environment for DFI due to both the slower combustion development of the main and the colder gas inside the duct retrieved by the tail of the main spray and pushed out by the tip of the post spray. In terms of soot mass, the soot formation mitigation provided by the duct, motivated in previous paragraphs, is evident: the difference between the two configurations is amplified in the bowl region; in fact, the soot is forming at a higher rate for free spray, as confirmed in Figure 8.
- **17 deg aTDCf**: This time instant relates to the combustion of the post injection. A cold path can be observed from the injector to the piston rim for DFI, making more evident the temperature reduction. This relatively cold gas brought from the duct into the combustion region further increases the ID associated with the post injection for DFI and tends to deteriorate the late combustion process, as shown in Figure 8 where the typical DFI faster burnout is not present. This slowdown of the post injection combustion is expected to also have a negative impact on soot oxidation. Looking at the soot mass distribution, the positive impact of DFI on the soot formation related to the main combustion is again evident. However, the soot pockets are moving back toward the duct region where soot oxidation can be more difficult. The soot formation due to post-injection-related combustion can also be observed close to the bowl lip for both free spray and DFI, with lower values of soot mass for DFI.
- **23 deg aTDCf**: This time instant is associated with the maximum in-cylinder soot mass. A temperature increase near the bowl lip can be observed for DFI due to the post injection combustion occurring later than free spray. On

FIGURE 12 Soot mass distribution on a vertical section of the combustion chamber for both free spray (top) and DFI (bottom) configuration at different time instants (from left to right). Working point: 1800 rpm at 6 bar.

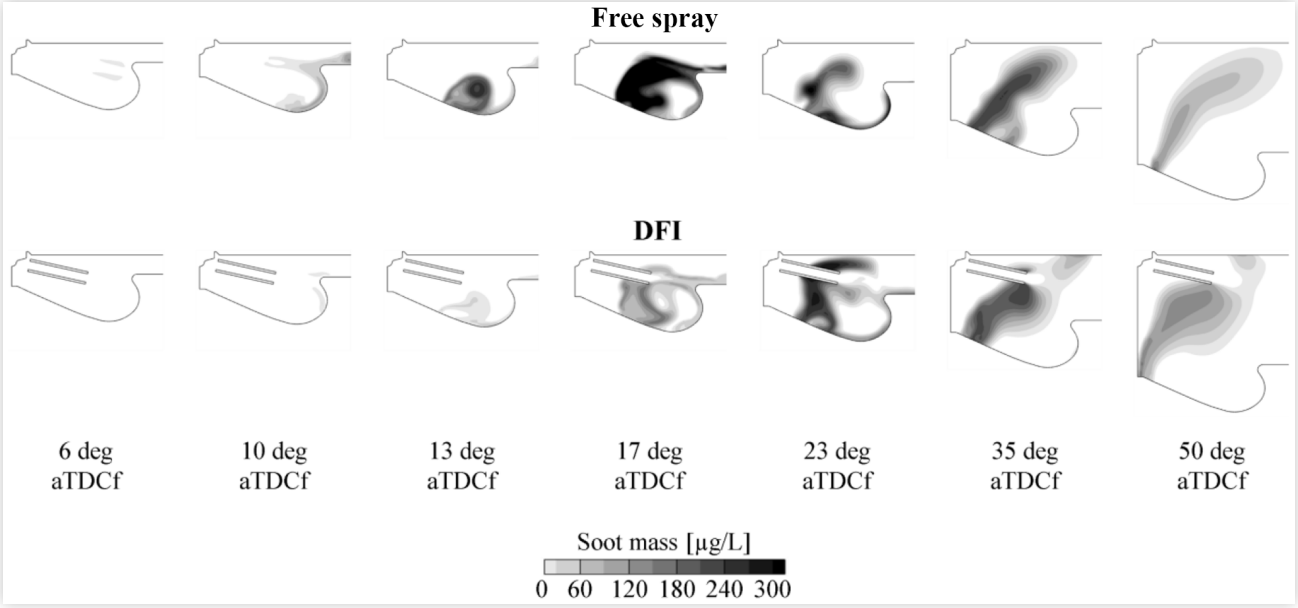

the contrary, the temperatures are generally lower for DFI in the rest of the volume, especially in the region occupied by the duct. These low-temperature areas (i.e., at about 1600–1800 K) are reflected as high-soot pockets on the soot distributions due to the reduced oxidation rate.

- **35 deg aTDCf**: This time instant is associated with the breakeven point between the soot traces in Figure 8; thus, free spray and DFI are characterized by an equal soot mass in the cylinder, but a different soot oxidation rate. Again, DFI features lower combustion temperature values, especially for the gases surrounding the duct volume, and a blue cold region inside the duct where combustion is not occurring. Therefore, the volume involved in the combustion process is smaller. As said above, the lower combustion temperature values work as a sort of tracer of high soot concentration regions due to the reduced oxidation. In fact, the highest soot mass values for DFI are reached close to the duct. The oxidation is inhibited in that region due to three main effects: first, the temperatures are lower; second, the soot on the duct wall cannot comes in direct contact with the oxidizing air; third, the duct presence acts as a sort of container, removing part of the available fresh air essential to oxidize the formed soot mass. Therefore, the free-spray case has a larger amount of air available for soot oxidation purposes. This aspect is particularly critical due to the reduced dimension of the chamber and due to the piston bowl design, which directs the spray toward the center, where the duct occupies most of the available space. This consideration suggests that a geometrical optimization of the combustion chamber could be of paramount importance for DFI implementation in light-duty diesel engines.
- **50 deg aTDCf**: This time instant is related to the late soot oxidation phase when DFI is characterized by a higher soot mass than free spray. DFI shows lower temperatures in the center of the chamber, where the duct is present, confirming that it is hindering the soot oxidation process. Both free spray and DFI feature a residual soot pocket near the bowl dome where a possible interaction could occur with the other sprays, especially for the DFI, due to the higher spray velocity. While the soot mass progressively reduces moving from the bowl to the cylinder head, another large soot pocket is present for DFI near the duct due to the mechanisms analyzed at the previous time instants.

Impact of Post Injection According to the analysis on the part-load working point, the direct retrofit approach for DFI seems not a viable solution for both engine calibration and engine design aspects. Indeed, although a soot reduction was observed during the formation phase, soot oxidation was strongly inhibited for DFI, leading to higher engine-out soot emissions. The purpose of this section is to preliminary investigate if a variation of the engine calibration, without any modification of the engine design, could be beneficial for DFI. In particular, a simple variation of the injection pattern was considered, based on the previous results. The post injection

is typically involved in CDC for both enhancing soot oxidation, due to enhanced mixing and temperature effects, and reducing soot formation, due to the lower main injection duration [45]. In this case, the post injection seemed not beneficial for DFI due to the very slow reaction rate, leading to late-combustion degradation and no beneficial effect on soot oxidation. Therefore, a test with a simplified injection was executed, suppressing the post injection and increasing the main injection duration, in order to maintain equal total injected fuel mass. In Figure 13, the fuel injection rate, the burn rate and in-cylinder pressure, the in-cylinder soot mass, and the soot formation/oxidation rate are reported for both free spray and DFI as a function of CA. For the soot mass trace, the results associated with the previous analysis involving the post injection are illustrated again with dashed lines to facilitate the comparison.

Focusing on the burn rate (Figure 13(b)), it is easy to notice that the impact of the longer main injection on the premixed combustion phase is much higher for DFI (blue), which shows a larger increment of the peak. In fact, a larger amount of fuel mass is involved in the premixed combustion regime with respect to the free spray (red), thus being more affected by the higher amount of fuel mass injected during the main. The late combustion is more rapid for both configurations when post injection is excluded, leading to an increment in load, which is higher for DFI (+2.2% on IMEP) than free spray (+1.4% on IMEP), leading to only a less-than-1% reduction in IMEP for DFI. However, also, in this case, DFI does not feature the typical faster burnout present in constant-volume conditions.

Looking at the in-cylinder soot mass (Figure 13(c)), in the free-spray case the post injection removal (solid line) causes an in-cylinder soot mass peak increment due to a higher soot formation rate, as highlighted in Figure 13(d). Therefore the presence of the post injection (dashed line) seems to reduce the jet-fuel-rich regions, according to the *split-flame* and *jet replenishment* concepts [45, 46, 47], thus reducing the soot formation. Since the DFI case reduces the soot mass enabling different mechanisms, the well-known effects of post injection on soot formation cannot be considered. Only a slight increment in the soot mass slope can be detected with a similar peak of the soot mass curve. In other words, during the soot formation phase, the removal of the post injection worsens the free-spray configuration, while it almost does not affect the DFI one. As far as the soot oxidation phase is concerned, the absence of post injection in the free-spray case causes a slightly steeper slope of the soot mass curve. However, the removal of the post injection leads to higher engine-out soot emissions at EVO, as expected. The outcome related to the DFI configuration is different: starting from a similar amount of soot mass formed, the slope of the curve associated with the injection strategy without post injection is remarkably steeper than the main plus post injection one. Hence, the engine-out soot emissions are reduced when the post injection is removed for the DFI case. In particular, comparing free spray and DFI without post injection, a 22% engine-out soot mass reduction can

FIGURE 13 Fuel injection rate (a), burn rate and in-cylinder pressure (b), in-cylinder soot mass (c), and soot formation/oxidation rate (d) for both free spray (red) and DFI (blue). Injection patterns without post injection (solid lines) and with post injection (dashed lines) are compared. Working point: 1800 rpm at 6 bar.

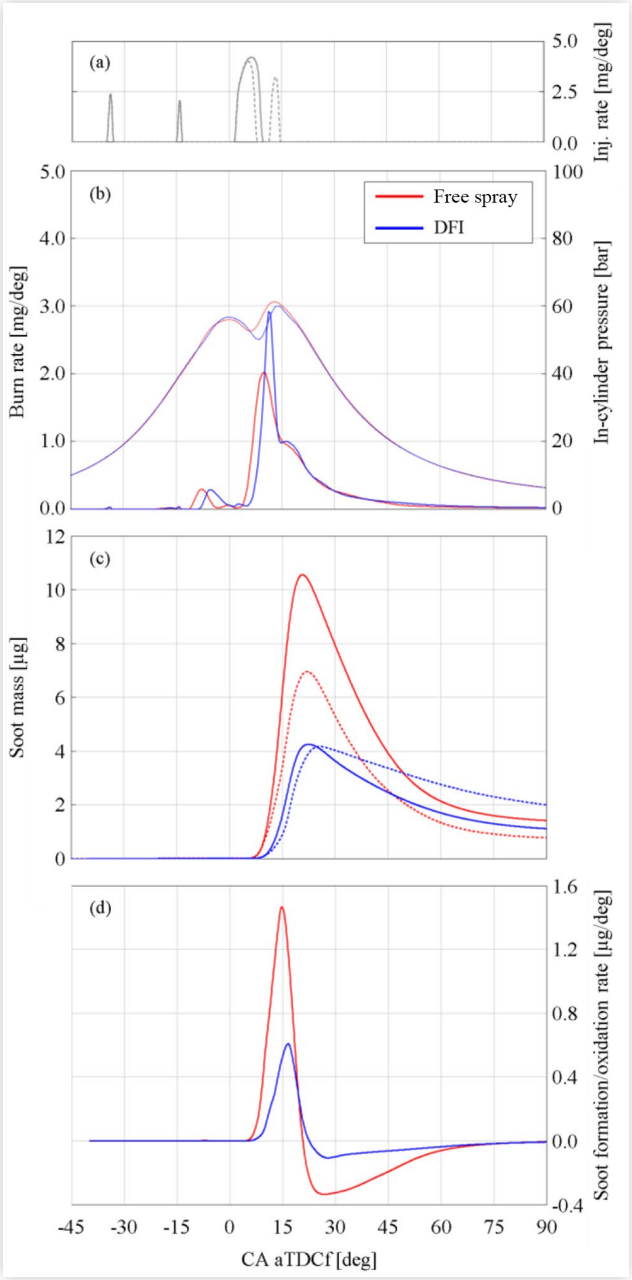

be observed with the adoption of the duct. It is noteworthy, that this outcome is achieved despite the limitation associated with the combustion chamber size and design, which are detrimental to soot oxidation with DFI, eroding its benefits in terms of soot formation.

Even though the suppression of the post injection was revealed to be very beneficial for DFI, at the current state the

lowest engine-out soot mass is still reached by the free spray with the initial calibration. However, from the present analysis, good potentialities emerge from DFI technology, which is able to achieve much lower soot formation and only slightly higher engine-out soot emissions compared to the free-spray reference curve. In fact, it has to be taken into account that no real effort was spent in optimizing the DFI combustion system and related calibration, maintaining a bowl design that has been demonstrated to partially deteriorate the DFI benefits. On the contrary, the free-spray case is the result of a time-consuming engine design and calibration optimization. In other words, a DFI-oriented calibration could lead to very interesting results for the DFI configuration, even in a light-duty retrofitted combustion chamber design. In addition, a DFI-oriented geometrical optimization of the chamber would further pave the way to its success as soot-curtailing technology for diesel combustion.

3.3. K-Point: 2800 rpm × Full Load

The results of the sector combustion simulations related to the full-load K-point are presented in this section, comparing free-spray and DFI configuration. In Figure 14, the fuel injection rate, the burn rate and in-cylinder pressure, the in-cylinder soot mass, and the soot formation/oxidation rate are reported for both free spray and DFI as a function of CA.

The injection strategy (Figure 14(a), gray) is based on a single and quite long main injection at about 2200 bar rail pressure. This strategy is the most comparable to the CVCV analyses in literature [14, 16, 18-20, 38, 41], but the differences related to the volume variation and the spray/bowl interaction must be taken into account.

Focusing on the burn rate (Figure 14(b)), it is easy to note a degradation in the combustion when the duct is used (blue solid line). Apart from the late combustion phase, the DFI features slower combustion than free spray (red) most of the time, without any ID increase. This is because DFI technology is not working properly due to ignition inside the duct. Indeed, a significant portion of the fuel burn rate occurs inside the duct for the whole injection duration, as reported on the same graph with a blue dotted line. In terms of in-cylinder pressure trace (Figure 14(b)), a large gap is present between free spray and DFI for the entire combustion duration, with a reduction of about 20 bar at the pressure peak for the latter. This is the effect of the combustion degradation previously highlighted, leading to a remarkable load reduction (-10% IMEP) at constant injected mass. For the sake of clarity, the in-duct combustion is also analyzed in terms of local temperature distribution a few instants after the ignition (at -2 deg aTDCf) for both the free and the ducted sprays on two different combustion chamber sections (Figure 15). As in Figure 9, the vertical section and the respective orthogonal section, passing for the nozzle axes, are considered.

From both sections, it can be observed how the combustion is established inside the duct (right) for approximately its entire length. In particular, focusing on the orthogonal

FIGURE 14 Fuel injection rate (a), burn rate and in-cylinder pressure (b), in-cylinder soot mass (c), and soot formation/oxidation rate (d) for both free spray (red) and DFI (blue). Working point: 2800 rpm at full load.

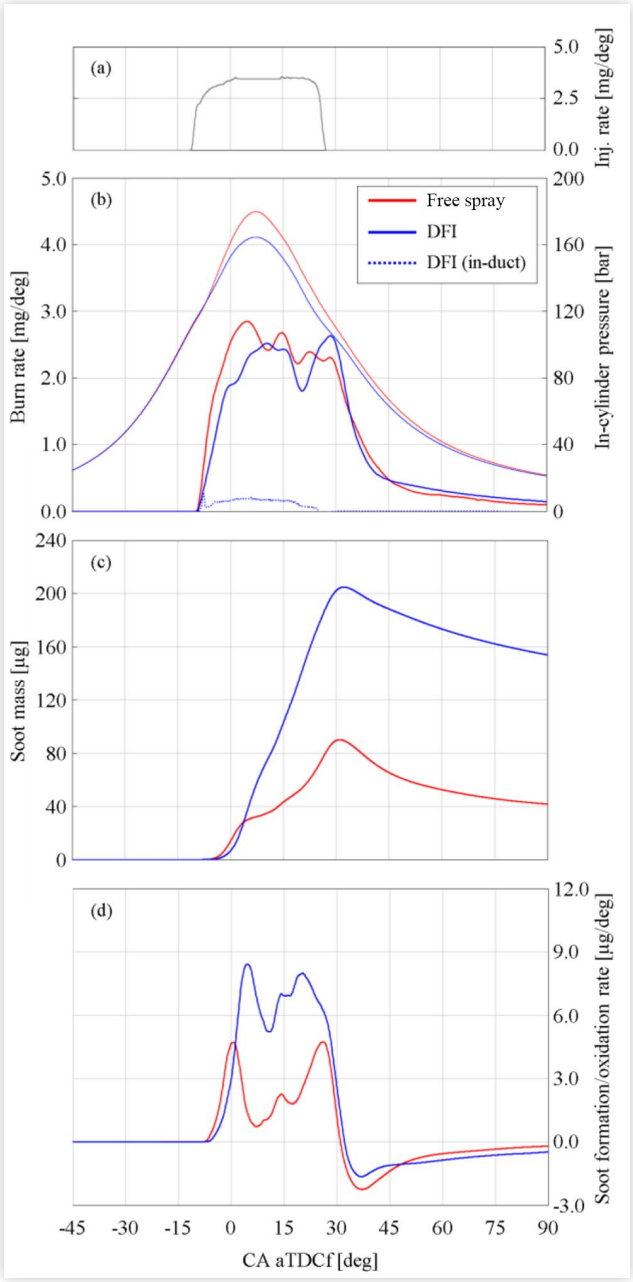

sections (A-A in Figure 15, bottom), the combustion is starting very close to the injector orifice exit for free spray (left) and an initial temperature rise is present even before the duct inlet for DFI. The very high reactivity conditions characteristics of the full load K-point are thus prohibitive for a proper DFI operation, as they are too prone to trigger in-duct combustion. These results are in line with previous work in constant-volume conditions [20]. In that case, the DFI benefits were limited by the in-duct combustion for air density values higher

FIGURE 15 Temperature distribution at –2 deg aTDCf on a vertical section (top) and a respective orthogonal section (A-A, bottom) of the combustion chamber for both free spray (left) and DFI (right). Working point: 2800 rpm at full load.

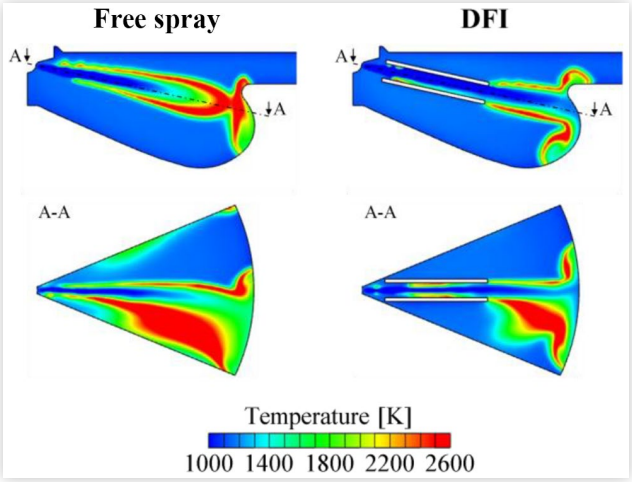

than 40 kg/m3, with an injector orifice diameter of 0.180 mm. In this case, considering the SOI injection timing, the in-cylinder average temperature and density are about 1030 K and 33 kg/m3, with a spray more prone to evaporation due to the lower injector orifice diameter (i.e., approximately 0.140 mm). Even though these conditions would be already critical if compared with the previous ones, the herein injected spray is subjected to even higher density and temperature values caused by the continuation of the compression stroke up to the TDCf and the beginning of the combustion. In addition, it can be interesting to analyze the shape of the flame on the orthogonal section: for the free-spray case, the flame largely deviates from the initial spray axis, partially going out of the sector due to the swirl motion effect; instead, for the DFI case, the spray axial direction is maintained due to both the swirl reduction (observed in Figure 6) and the higher momentum of the spray exiting the duct. Although the swirl reduction could have a negative impact in terms of soot oxidation, the shape of the DFI flame here observed could be beneficial to mitigate the jet-jet interaction, among the main sources of soot in diesel combustion [48, 49, 50].

Moving to the soot mass (Figure 14(c)), the in-duct combustion causes a much higher in-cylinder soot mass for DFI during both formation and oxidation phases, as found in both experimental [14, 16] and numerical [19, 20] research available in the literature. In fact, the soot formation mitigation mechanisms enabled by the duct adoption are deteriorated due to the in-duct ignition. On one hand, the in-duct combustion causes a pressure increment inside the duct, reducing the pumping effect that acts as a driver of the duct-enabled upstream entrainment. On the other hand, the turbulent mixing inside and downstream of the duct, which occurs after the contact between the spray and duct wall due to high-velocity gradients, is practically nullified since the LOL is shorter than the contact distance. Therefore, the absence of these mechanisms combined with a reduced oxidation potential due to the presence of the duct wall, inhibiting the contact with the surrounding air, causes the herein much higher soot formation rate (Figure 14(d)) for DFI.

In conclusion, the present investigation on a full-load working point of an existing CI engine highlights that the adoption of the duct with a direct retrofit approach could not be possible due to different engine calibration requirements between free spray and DFI. In particular, this and previous analyses [20, 23, 25] highlighted that DFI technology suffers some critical areas of the engine operating map when high density–high temperature conditions are achieved. In fact, the risk of in-duct combustion grows, making DFI not only to be not beneficial but even worsening the CDC outcome.

4. Conclusions

The aim of this study was to numerically investigate the potential of DFI implementation in a CI engine for light-duty applications, highlighting the factors which can limit or facilitate its integration in existing combustion chambers. For this purpose, a 1D/3D-CFD coupling methodology was employed to develop an engine model, validated against experimental data coming from the test bench for three different working points. The model validation was executed for the free-spray configuration. This engine model was then employed to assess the DFI technology compared to the free spray in terms of the main combustion parameters, in-cylinder soot mass, and physical mechanisms associated with soot reduction.

From the cold flow analysis, it emerged that the presence of the ducts inside the cylinder has a significant impact on both the velocity and thermal fields. On one hand, it tends to attenuate the typical fluid bulk motions of diesel engines (like the swirl), having a possible impact on the mixing mechanisms exploited to decrease soot emissions in diesel combustion chambers. On the other hand, the duct wall regime temperature largely affects the local temperature conditions encountered by the spray at the start of injection, suggesting that duct thermal management plays a crucial role. The combustion analysis was then carried out on both part-load (engine speed 1800 rpm; BMEP 6 bar) and full-load working points (engine speed 2800 rpm; BMEP about 23 bar). The most important conclusions coming from this study are reported below.

Part Load

- DFI was capable of remarkably attenuating soot formation due to the equivalence ratio reduction. In this case study, it was mainly driven by the charge gas entrainment enhancement at the duct inlet and by the LOL extension, while the DFI effect on the turbulent mixing was mitigated, probably because of the lower jet liquid fraction with respect to previous studies.

- In this light-duty engine configuration characterized by a re-entrant bowl shape, DFI suffered soot oxidation since the formed soot mass was directed toward the duct region where lower temperatures and lower air availability drastically reduced the oxidation potential.
- The employed injection strategy, optimized for CDC, seems not straightforward for DFI, which is shown to work better without post injection. In fact, the slower reaction rate associated with the post injection led to the degradation of DFI late combustion.

Full Load

- The high density–high temperature conditions typical of a full-load working point are prohibitive for the DFI configuration due to the occurrence of in-duct combustion. This detrimental operation must be absolutely avoided to conserve the duct-enabled soot mitigation mechanisms; otherwise, higher engine-out soot emissions are expected for DFI.
- A limit on the engine operating map or a DFI-oriented design of the combustion system seems needed to exploit DFI benefits at high-load working points.

In conclusion, the direct retrofit of existing light-duty CI engines, employing a similar spray-targeted combustion chamber design, seems not a viable solution for DFI, at least if an engine calibration optimized for CDC is considered. However, a simple variation of the injection pattern (in the part-load analysis) made it emerge a great potential if consistent efforts will be spent on a DFI-oriented engine recalibration. Furthermore, simultaneous DFI-oriented optimization of the combustion chamber geometry would allow exploiting the reported remarkable soot formation reduction with DFI, reducing the oxidation penalties due to the present spray/wall interaction outcome. In particular, according to the present results, it can be speculated that the *simplification*, for both engine calibration and design, could be a valuable path to pursue toward the success of the DFI technology.

Acknowledgment

Computational resources were provided by HPC@POLITO, a project of the Academic Computing Center in the Department of Control and Computer Engineering at the Politecnico di Torino (http://www.hpc.polito.it). This work is based on an oral presentation given at the SAE International 2022 WCX™ World Congress Experience.

Contact Information

Andrea Piano, PhD
Politecnico di Torino | Energy Department (DENERG)
Corso Duca degli Abruzzi, 24 | 10129 Torino (IT)
Tel: +39 011 0904563
andrea.piano@polito.it

Abbreviations

AMR - Adaptive Mesh Refinement
aTDCf - after Top Dead Center firing
BMEP - Brake Mean Effective Pressure
CA - Crank Angle
CDC - Conventional Diesel Combustion
CFD - Computational Fluid Dynamics
CI - Compression-Ignition
CO_2 - Carbon dioxide
CR - Compression Ratio
CVCV - Constant-Volume Combustion Vessel
D - Duct diameter
DFI - Ducted Fuel Injection
ECN - Engine Combustion Network
EVO - Exhaust Valve Opening
G - Stand-off distance
ID - Ignition Delay
IMEP - Indicated Mean Effective Pressure
IVC - Intake Valve Closure
L - Duct length
LL - Liquid Length
LLFC - Leaner Lifted-Flame Combustion
LOL - Lift-Off Length
MC - Mixing-Controlled
MFB - Mass Fraction Burned
NL - Natural Luminosity
NOx - Nitrogen Oxides
PN - Particulate Number
RANS - Reynolds-Averaged Navier-Stokes
SOI - Start of Injection
TDC - Top Dead Center
TKE - Turbulent Kinetic Energy
ϕ - Equivalence ratio

References

1. Fortune Business Insight, "Marine Engine Market Size," 2021.
2. ACEA, "New Trucks in the EU by Fuel Type," 2021, https://www.acea.auto/figure/trucks-eu-fuel-type/, accessed April 2022.
3. Miller, J. and Jin, L., "Global Progress toward Soot-Free Diesel Vehicles in 2019," International Council on Clean Transportation (ICCT), 2019.

4. Klimont, Z., Kupiainen, K., Heyes, C., Purohit, P. et al., "Global Anthropogenic Emissions of Particulate Matter Including Black Carbon," *Atmos. Chem. Phys.* 17 (2017): 8681-8723, doi:10.5194/acp-17-8681-2017.
5. Anenberg, S.C., Schwartz, J., Shindell, D., Amann, M. et al., "Global Air Quality and Health Co-Benefits of Mitigating Near-Term Climate Change through Methane and Black Carbon Emission Controls," *Environ. Health Perspect.* 120, no. 6 (2012): 831-839, doi:10.1289/ehp.1104301.
6. Anenberg, S., Miller, J., Henze, D., and Minjares, R., *A Global Snapshot of the Air Pollution-Related Health Impacts of Transportation Sector Emissions in 2010 and 2015* (Washington, DC: International Council Clean Transportation, 2019)
7. Janssen, N.A., Gerlofs-Nijland, M.E., Lanki, T., Salonen, R.O. et al., "Health Effects of Black Carbon," WHO, 2012.
8. Bond, T.C., Doherty, S.J., Fahey, D.W., Forster, P.M. et al., "Bounding the Role of Black Carbon in the Climate System: A Scientific Assessment," *J. Geophys. Res. Atmos.* 118 (2013): 5380-5552, doi:10.1002/jgrd.50171.
9. ICCT, "Vision 2050: A Strategy to Decarbonize the Global Transport Sector by Mid-Century," 2020, ISBN:978-4-431-09430-2.
10. Skeen, S., Manin, J., Pickett, L., Cenker, E. et al., "A Progress Review on Soot Experiments and Modeling in the Engine Combustion Network (ECN)," *SAE Int. J. Engines* 9, no. 2 (2016): 883-898, doi:10.4271/2016-01-0734.
11. Gehmlich, R., Dumitrescu, C., Wang, Y., and Mueller, C., "Leaner Lifted-Flame Combustion Enabled by the Use of an Oxygenated Fuel in an Optical CI Engine," *SAE Int. J. Engines* 9, no. 2 (2016): 883-898, doi:https://doi.org/10.4271/2016-01-0730.
12. Polonowski, C., Mueller, C., Gehrke, C., Bazyn, T. et al., "An Experimental Investigation of Low-Soot and Soot-Free Combustion Strategies in a Heavy-Duty, Single-Cylinder, Direct-Injection, Optical Diesel Engine," *SAE Int. J. Fuels Lubr.* 5, no. 1 (2012): 51-77, doi:https://doi.org/10.4271/2011-01-1812.
13. Mueller, C.J., Ducted fuel injection. U.S. Patent 9,909,549 B2, 2018.
14. Mueller, C.J., Nilsen, C.W., Ruth, D.J., Gehmlich, R.K. et al., "Ducted Fuel Injection: A New Approach for Lowering Soot Emissions from Direct-Injection Engines," *Appl. Energy* 204 (2017): 206-220, doi:10.1016/j.apenergy.2017.07.001.
15. Engine Combustion Network (ECN), "Diesel Spray Combustion," 2019, https://ecn.sandia.gov/diesel-spray-combustion/, accessed April 2022.
16. Gehmlich, R.K., Mueller, C.J., Ruth, D.J., Nilsen et al., "Using Ducted Fuel Injection to Attenuate or Prevent Soot Formation in Mixing-Controlled Combustion Strategies for Engine Applications," *Appl. Energy* 226 (2018): 1169-1186, doi:10.1016/j.apenergy.2018.05.078.
17. Nilsen, C., Yraguen, B., Mueller, C., Genzale, C. et al., "Ducted Fuel Injection vs. Free-Spray Injection: A Study of Mixing and Entrainment Effects Using Numerical Modeling," *SAE Int. J. Engines* 13, no. 5 (2020): 705-715, doi:https://doi.org/10.4271/03-13-05-0044.
18. Millo, F., Piano, A., Peiretti Paradisi, B., Postrioti, L. et al., "Ducted Fuel Injection: Experimental and Numerical Investigation on Fuel Spray Characteristics, Air/Fuel Mixing and Soot Mitigation Potential," *Fuel* 289 (2021): 119835, doi:10.1016/j.fuel.2020.119835.
19. Millo, F., Piano, A., Peiretti Paradisi, B., Segatori, C. et al., "Ducted Fuel Injection: A Numerical Soot-Targeted Duct Geometry Optimization," *SAE Int. J. Engines* 15, no. 2 (2022): 297-317, doi:https://doi.org/10.4271/03-15-02-0014.
20. Millo, F., Segatori, C., Piano, A., Peiretti Paradisi, B. et al., "An Engine Parameters Sensitivity Analysis on Ducted Fuel Injection in Constant Volume Vessel Using Numerical Modeling," SAE Technical Paper 2021-24-0015, 2021, https://doi.org/10.4271/2021-24-0015.
21. Nilsen, C., Biles, D., and Mueller, C., "Using Ducted Fuel Injection to Attenuate Soot Formation in a Mixing-Controlled Compression Ignition Engine," *SAE Int. J. Engines* 12, no. 3 (2019): 309-322, doi:https://doi.org/10.4271/03-12-03-0021.
22. Nilsen, C., Biles, D., Yraguen, B., and Mueller, C., "Ducted Fuel Injection versus Conventional Diesel Combustion: An Operating-Parameter Sensitivity Study Conducted in an Optical Engine with a Four-Orifice Fuel Injector," *SAE Int. J. Engines* 3, no. 3 (2020): 345-362, doi:https://doi.org/10.4271/03-13-03-0023.
23. Nilsen, C., Biles, D., Yraguen, B., and Mueller, C., "Ducted Fuel Injection vs. Conventional Diesel Combustion: Extending the Load Range in an Optical Engine with a Four-Orifice Fuel Injector," *SAE Int. J. Engines* 14, no. 1 (2021): 47-58, doi:https://doi.org/10.4271/03-14-01-0004.
24. Wilmer, B.M., Nilsen, C.W., Biles, D.E., Mueller, C.J. et al., "Solid Particulate Mass and Number from Ducted Fuel Injection in an Optically Accessible Diesel Engine in Skip-Fired Operation," *Int. J. Engine Res.* 23, no. 7 (2022): 1226-1236, doi:10.1177/14680874211010560.
25. Svensson, K., Kim, C., Seiler, P., Martin, G. et al., "Performance and Emission Results from a Heavy-Duty Diesel Engine with Ducted Fuel Injection," SAE Technical Paper 2021-01-0503, 2021, https://doi.org/10.4271/2021-01-0503.
26. Millo, F., Piano, A., Peiretti Paradisi, B., Marzano, M.R. et al., "Development and Assessment of an Integrated 1D-3D CFD Codes Coupling Methodology for Diesel Engine Combustion Simulation and Optimization," *Energies* 13, no. 7 (2020): 1612, doi:10.3390/en13071612.
27. Amsden, A.A., O'Rourke, P.J., and Butler, T.D., "KIVA-II: A Computer Program for Chemically Reactive Flows with Sprays," Los Alamos National Lab. (LANL), Los Alamos, NM, 1989.
28. Puri Lng, T., Soni Lng, L., and Deshpande, S., "Combined Effects of Injection Timing and Fuel Injection Pressure on Performance, Combustion and Emission Characteristics of a Direct Injection Diesel Engine Numerically Using CONVERGE CFD Tool," SAE Technical Paper 2017-28-1953, 2017, https://doi.org/10.4271/2017-28-1953.
29. Yakhot, V. and Orszag, S.A., "Renormalization Group Analysis of Turbulence. I. Basic Theory," *J. Sci. Comput.* 1 (1986): 3-51, doi:10.1007/BF01061452.

30. Reitz, R. and Diwakar, R., "Structure of High-Pressure Fuel Sprays," SAE Technical Paper 870598, 1987, https://doi.org/10.4271/870598.
31. Reitz, R.D. and Bracco, F.V., "Mechanisms of Breakup of Round Liquid Jets," *Encyclopedia of Fluid Mechanics* (Houston, TX: Gulf Publishing Company, 1986).
32. Liu, A., Mather, D., and Reitz, R., "Modeling the Effects of Drop Drag and Breakup on Fuel Sprays," SAE Technical Paper 930072, 1993, https://doi.org/10.4271/930072.
33. Naber, J. and Reitz, R., "Modeling Engine Spray/Wall Impingement," SAE Technical Paper 880107, 1988, https://doi.org/10.4271/880107.
34. Amsden, A.A. and Findley, M., "KIVA-3V: A Block-Structured KIVA Program for Engines with Vertical or Canted Valves," Lawrence Livermore National Lab. (LLNL), Livermore, CA, 1997.
35. Richards, K.J., Senecal, P.K., and Pomraning, E., CONVERGE 2.4, Convergent Science, Madison, WI, 2018.
36. Zeuch, T., Moréac, G., Ahmed, S.S., and Mauss, F., "A Comprehensive Skeletal Mechanism for the Oxidation of n-Heptane Generated by Chemistry-Guided Reduction," *Combust. Flame* 115 (2008): 651-674, doi:10.1016/j.combustflame.2008.05.007.
37. Kazakov, A. and Frenklach, M., "Dynamic Modeling of Soot Particle Coagulation and Aggregation: Implementation with the Method of Moments and Application to High-Pressure Laminar Premixed Flames," *Combust. Flame* 114 (1998): 484-501, doi:10.1016/S0010-2180(97)00322-2.
38. Fitzgerald, R., Svensson, K., Martin, G., Qi, Y. et al., "Early Investigation of Ducted Fuel Injection for Reducing Soot in Mixing-Controlled Diesel Flames," *SAE Int. J. Engines* 11, no. 6 (2018): 817-833, doi:https://doi.org/10.4271/2018-01-0238.
39. Li, F., Lee, C.f., Wu, H., Wang, Z. et al., "An Optical Investigation on Spray Macroscopic Characteristics of Ducted Fuel Injection," *Exp. Therm. Fluid Sci.* 109 (2019): 109918, doi:10.1016/j.expthermflusci.2019.109918.
40. Ong, J.C., Zhang, M., Jensen, M.S., and Walther, J.H., "Large Eddy Simulation of Soot Formation in a Ducted Fuel Injection Configuration," *Fuel* 313 (2022): 122735, doi:10.1016/j.fuel.2021.122735.
41. Svensson, K. and Martin, G., "Ducted Fuel Injection: Effects of Stand-Off Distance and Duct Length on Soot Reduction," *SAE Int. J. Adv. & Curr. Prac. in Mobil.* 1, no. 3 (2019): 1074-1083, doi:https://doi.org/10.4271/2019-01-0545.
42. Eismark, J., Andersson, M., Christensen, M., Karlsson, A. et al., "Role of Piston Bowl Shape to Enhance Late-Cycle Soot Oxidation in Low-Swirl Diesel Combustion," *SAE Int. J. Engines* 12, no. 3 (2019): 233-249, doi:https://doi.org/10.4271/03-12-03-0017.
43. Rhim, D. and Farrell, P., "Characteristics of Air Flow Surrounding Non-Evaporating Transient Diesel Sprays," SAE Technical Paper 2000-01-2789, 2000, https://doi.org/10.4271/2000-01-2789.
44. Fitzgerald, R., Svensson, K., and Martin, G., "Mixture Fraction Measurements of Diesel Sprays with Ducted Fuel Injection," *Int. Conf. Liq. At. Spray Syst.* 1, no. 1 (2021), doi:10.2218/iclass.2021.5939.
45. O'Connor, J. and Musculus, M., "Post Injections for Soot Reduction in Diesel Engines: A Review of Current Understanding," *SAE Int. J. Engines* 6, no. 1 (2013): 400-421, doi:https://doi.org/10.4271/2013-01-0917.
46. Desantes, J., Arrègle, J., López, J., and García, A., "A Comprehensive Study of Diesel Combustion and Emissions with Post-Injection," SAE Technical Paper 2007-01-0915, 2007, https://doi.org/10.4271/2007-01-0915.
47. Han, Z., Uludogan, A., Hampson, G., and Reitz, R., "Mechanism of Soot and NOx Emission Reduction Using Multiple-Injection in a Diesel Engine," SAE Technical Paper 960633, 1996, https://doi.org/10.4271/960633.
48. Genzale, C., Reitz, R., and Musculus, M., "Effects of Piston Bowl Geometry on Mixture Development and Late-Injection Low-Temperature Combustion in a Heavy-Duty Diesel Engine," *SAE Int. J. Engines* 1, no. 1 (2009): 913-937, doi:https://doi.org/10.4271/2008-01-1330.
49. Pickett, L. and López, J., "Jet-Wall Interaction Effects on Diesel Combustion and Soot Formation," SAE Technical Paper 2005-01-0921, 2005, https://doi.org/10.4271/2005-01-0921.
50. Chartier, C., Aronsson, U., Andersson, Ö., Egnell, R. et al., "Influence of Jet-Jet Interactions on the Lift-Off Length in an Optical Heavy-Duty DI Diesel Engine," *Fuel* 112 (2013): 311-318, doi:10.1016/j.fuel.2013.05.021.